Performance Potential of 2D Kagome Lattice Interconnects

Tong Wu and Jing Guo

***Abstract*— Kagome lattice materials are layered two-dimensional (2D) materials in which atoms are arranged in a trihexagonal tiling lattice pattern. It has been suggested that the Kagome lattice can possess topologically non-trivial band structures. By performing atomistic quantum transport simulations, we show that the topological edge modes of a Fe_3Sn Kagome nanoribbon have excellent carrier transport properties, with a mean free path several orders of magnitude larger than that of the bulk modes. Vertical stacking of intercalated Kagome layers can further boost the conductance per unit width. As a result, the 2D Kagome lattice materials offer low resistivity and promising potential for interconnect applications in the sub-10nm regime.**

***Index Terms*— Interconnect, topological insulator, kagome lattice.**

I. Introduction

AS COPPER interconnects continue to scale down, their resistivity increases significantly [1]. The interconnect RC delay degrades and becomes an increasing larger portion in the overall delay of the integrated circuits. To search for alternative interconnects with lower resistivity, carbon nanotubes and graphene nanoribbons have previously been proposed [2], [3]. However, carbon nanotubes can have variability in terms of mixture of metallic and semiconducting tubes. A narrow graphene nanoribbon, regardless of its chirality, always has a bandgap due to quantum confinement, edge bond relaxation or electron-electron interaction at the edges [4]. Furthermore, edge roughness lowers its conductivity as the width is scaled down.

It has been demonstrated experimentally that certain two-dimensional (2D) Kagome lattice materials can have topologically non-trivial electronic bands [5]. The Kagome monolayer lattice materials M_3X can be formed out of elements M and X, where the examples are M = Fe, Mn and X = Ge, Sn [5]–[7]. Theoretical studies have also shown that the Kagome lattice materials can be 2D topological insulators [8]. In a topological insulator, the edge modes are protected from backscattering, which can lead to excellent carrier transport properties. In this letter, the conductivity and transport properties of a 2D Kagome material are examined by atomistic quantum transport simulations. The results indicate that in the sub-10 nm regime, the Kagome lattice material can outperform Cu interconnects in terms of lower resistivity and have excellent potential for future interconnect applications.

Manuscript received August 24, 2019; revised September 27, 2019; accepted October 7, 2019. Date of publication October 14, 2019; date of current version November 27, 2019. This work was supported by NSF awards under Grant 1904580, Grant 1809770, and Grant 1618762. The review of this letter was arranged by Editor A. J. Naeemi. *(Corresponding author: Jing Guo.)*

The authors are with the Department of Electrical and Computer Engineering, University of Florida, Gainesville, FL 32611 USA (e-mail: guoj@ufl.edu).

Color versions of one or more of the figures in this letter are available online at http://ieeexplore.ieee.org.

Digital Object Identifier 10.1109/LED.2019.2947285

II. Approach

Monolayer Fe_3Sn has a 2D Kagome lattice structure, as shown in Fig. 1(a), in which Fe atoms occupy the triangular-shaped corners of the hexagons and form a trihexagonal tiling pattern, and the Sn atoms occupy the centers of the hexagons. The electronic structure near the Fermi level is due to the Fe atoms, and the bond part of a tight-binding Hamiltonian can be expressed as [5], [8],

$$H_B = -t_0 \sum_{\langle i,j \rangle} c_i^+ c_j, \tag{1}$$

where t_0 is the nearest-neighbor hopping parameter between the sites $\langle i, j \rangle$. The spin-orbit coupling (SOC) Hamiltonian can be described in a tight-binding form with an imaginary nearest-neighbor binding parameter [5],

$$H_{SOC} = i \sum_{\langle i,j \rangle} \lambda_{ij} \left(c_{i\uparrow}^+ c_{j\uparrow} - c_{i\downarrow}^+ c_{j\downarrow} \right), \tag{2}$$

where $\uparrow$ and $\downarrow$ are spin indices, $\lambda_{ij} = \lambda_0 \left(\hat{E}_{ij} \times \hat{R}_{ij} \right) \cdot \hat{s}$, $\hat{E}_{ij}$ is the directional vector of the in-plane electric field, $\hat{R}_{ij}$ is the bond directional vector, and $\hat{s}$ is the Pauli operator for electron spin, and λ_0 is the SOC strength parameter. The above form of SOC Hamiltonian results in a SOC term in the Kane-Mele type [9]. Without considering the SOC effect, the Hamiltonian H_B in Eq. (1) results in a flat band and a pair of gapless Dirac bands crossing at the K and K' points of the Brillouin zone. By considering the SOC effect $H = H_B + H_{SOC}$, a band gap of $E_g = 2\sqrt{3}\lambda_0$ opens at the Dirac points. The E-k relation near the intrinsic Fermi level can be expressed in a form of dispersive Dirac Fermions,

$$E(k) = \pm\sqrt{(\hbar v_F k)^2 + \left(E_g/2\right)^2}, \tag{3}$$

where $\hbar$ is the reduced Planck constant and the velocity parameter is $v_F = \sqrt{3}at_0/\hbar$. Here, we use the material parameters for the Fe_3Sn monolayer Kagome lattice given in [5]. The in-plane lattice constant as shown in Fig. 1(a) is $a = 0.5338$ nm, the tight binding parameter is $t_0 \approx 123$ meV, which results in $v_F \approx 1.85 \times 10^5$ m/s. The SOC parameter $\lambda_0 \approx 9.24$ meV, which results in a bandgap $E_g \approx 32$ meV and a ratio of $\lambda_0/t_0 \approx 0.075$. The monolayer Fe_3Sn can be intercalated by Stanene layers and forms a vertical stack, with a vertical lattice constant of $c \approx 1.5$ nm, as shown in Fig. 1(b) [5].

By patterning the 2D Kagome lattice to nanometer-width, Kagome lattice nanoribbons can be formed. The edge atoms

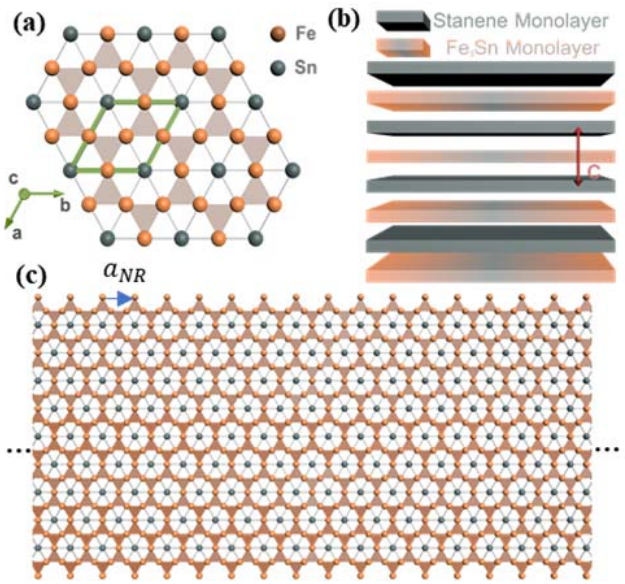

Fig. 1. (a) 2D monolayer Kagome lattice structure. (b) Schematic stack of Fe_3Sn monolayers intercalated by Stanene layers. (c) A monolayer Kagome nanoribbon with armchair-shaped edges.

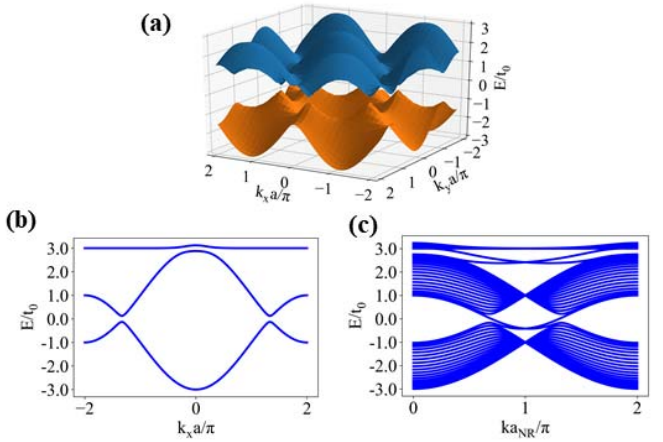

Fig. 2. (a) Band structure of a 2D Fe_3Sn lattice with SOC. The energy is normalized to the binding parameter t_0. (b) 2D band structure viewed along k_X direction at $k_Y = 0$. (c) The calculated band structure of a armchair edge Fe_3Sn nanoribbon with $n = 20$, which has a width of $W = \sqrt{3}na/2 \approx 9.25nm$.

are passivated by H atoms, so that no dangling bonds exist at the edges. Fig. 1(c) shows a Kagome nanoribbon with an armchair-shaped edge. The nanoribbon has a lattice constant of $a_{NR} = a \approx 0.5338$ nm along the length direction and a nanoribbon width of $W = \sqrt{3}na/2$, where n is an integer.

To study the carrier transport properties of the nanoribbon, the non-equilibrium Green's function (NEGF) formalism is used with the tight binding Hamiltonian as described above. The modeled nanoribbon has a scattering region of length L, with semi-infinite nanoribbon contacts on both ends. To study the effect of short-range scattering mechanisms such as defects on the conductivity and transport properties, a Gaussian random atomic potential is introduced at each atomic site of the scattering region. The short-range scattering potential is assumed to have a mean value of zero and a standard deviation of δV_a. By statistically averaging over hundreds of random realizations of the scattering potential, the average transmission is calculated, and the conductance can be obtained from the statistically averaged transmission by using the Landauer-Buttiker formula [10]. For the edge modes in a nanoribbon, backscattering due to long-range scattering mechanisms, such as charge impurity scattering and acoustic phonon scattering, is suppressed and has a weaker effect than the short-range scattering mechanisms due to considerations of momentum conservation and symmetry, which is neglected for simplicity. Room temperature $T = 300K$ is assumed in this study.

III. Results

Fig. 2(a) shows the dispersive Dirac bands of monolayer Fe_3Sn, in which the direct bandgap is located at the corners of the hexagonal Brillouin zone, and is proportional to the spin-orbit coupling strength. The unit cell of the Kagome lattice has three atoms. In addition to these two dispersive Dirac bands, there is an additional nearly flat band as shown in Fig. 2(b). The intrinsic Fermi level, located at the middle of the dispersive Dirac gap, is taken as energy zero. Fig. 2(c) shows the band structure of a Kagome nanoribbon with an armchair-shaped edge as shown in Fig. 1(c). For the nanoribbon, a pair of edge bands crosses the entire band gap energy range. The bands do not exist in the 2D bulk band structure. Examination of the calculated wave function confirms that these bands are spatially located at the edges of the nanoribbon.

Carrier transport properties of the Kagome nanoribbons are studied next by using the NEGF transport simulations. Fig. 3(a) shows the simulated transmission vs. energy in the presence of scattering compared to that at the ballistic limit. The standard deviation of the Gaussian distribution of the scattering potential $\Delta U_a = 4\lambda_0$ is larger than the 2D Kagome lattice bandgap $E_g = 2\sqrt{3}\lambda_0$. The ballistic transmission shows a clear stepwise feature, with the steps at the subband edges. In the bandgap region, the ballistic transmission is 1 due to the edge modes as shown in Fig 2. In the presence of scattering, the edge modes are topologically protected from backscattering and the transmission is still close to 1. In contrast, the transmission for the bulk modes is severely degraded. To quantify the difference between the edge modes and other modes, the average carrier scattering mean free path $\langle\lambda(E)\rangle$ can be extracted from the ratio of transmission with scattering $\langle T_S(E)\rangle$ and that at the ballistic limit $T_B(E)$ [10],

$$\frac{\langle T_S(E)\rangle}{T_B(E)} = \frac{\langle\lambda(E)\rangle}{L + \langle\lambda(E)\rangle}, \tag{4}$$

or equivalently, $\langle\lambda(E)\rangle = L/\left[T_B(E)/\langle T_S(E)\rangle - 1\right]$, where $\langle\cdot\rangle$ denotes average over random scattering potential samples for the quantity.

Fig. 3(b) shows the extracted mean free path $\lambda(E)$ vs. energy. The results indicate that the mean free path of the edge bands is over two order of magnitude larger than that of the bulk bands. Even in the presence of atomic scattering potential strength comparable to the bandgap value, the mean free path of the edge modes can be well above a micrometer.

The excellent carrier transport properties of the edge modes of the Kagome nanoribbons make them attractive for scaled interconnect applications. A major challenge of scaled

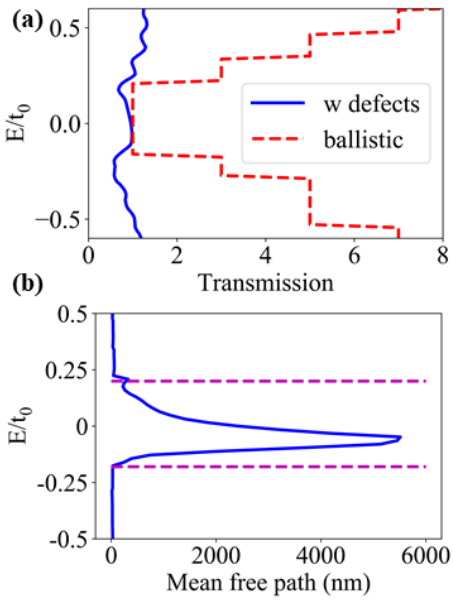

Fig. 3. (a) Transmission vs. energy at ballistic transport (dashed line) and in the presence of atomic scattering potential (solid line) by NEGF simulations, calculated over 200 random scattering potential realizations. The scattering potential has a Gaussian distribution with a mean of zero and standard deviation of $\Delta U_q = 4\lambda_0$ at all atom sites. The simulated ribbon has a width of $W = \sqrt{3}na/2 \approx 9.25nm$ for $n = 20$, and the scattering region has a length of $L = ma \approx 107$nm, where $m = 200$. (b) The extracted scattering mean free path vs. energy. The dashed lines show the nanoribbon bandgap energy range, within which the conductance is completely due to the edge bands.

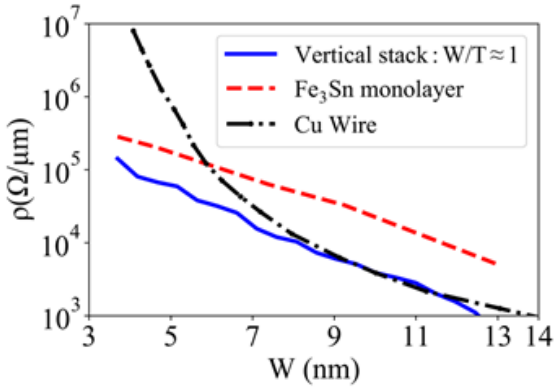

Fig. 4. Resistivity vs the width for interconnects made of monolayer Fe_3Sn nanoribbon, stacked nanoribbon layers as shown in Fig. 1(b), and Cu wire.

interconnects is to achieve low resistivity. The resistivity of a nanoribbon can be calculated from the mean free path $\langle\lambda(E)\rangle$ as,

$$\rho_{mo} = \left[\frac{q^2}{h}\int \langle\lambda(E)\rangle\left(-\frac{\partial f(E)}{\partial E}\right)dE\right]^{-1}, \qquad (5)$$

where q is the elementary electron charge, h is the Planck constant and $f(E) = 1/\left[1 + exp\left(\frac{E-E_F}{k_BT}\right)\right]$ is the Fermi-Dirac distribution function and E_F is the Fermi energy level. Fig. 4 shows the resistivity vs. the width of the monolayer nanoribbon compared to that of Cu wire [3], [11]. For a width smaller than 6nm, the Kagome monolayer nanoribbon outperforms the Cu wire in terms of lower resistivity. A vertical stack as shown in Fig. 1(b) can have multiple edge modes in parallel. By assuming a vertical stacking with an aspect ratio of W/T $\approx$ 1, the number of monolayers in a square wire can be approximately computed as, $n_L = [T/c] \approx [W/c]$ and the resistivity value becomes $\rho_w = \rho_{mo}/n_L$, where $[x]$ denotes the closest integer to x and ρ_{mo} is the resistivity of the monolayer. Below a width of 10nm, the stacked Kagome wire can offer better conductivity compared to the Cu wire with the same cross-sectional size. The advantage is especially significant as the size further scales down, while Cu wire suffers from significant increase of resistivity while the edge modes of the Kagome nanoribbons have much more preferred scaling properties.

IV. Conclusion

Atomistic quantum transport simulations are performed to investigate the carrier transport properties of the Kagome lattice nanoribbons. The results indicate that the edge modes maintain excellent carrier transport properties with mean free path orders of magnitude longer than other modes in the presence of scattering. Another advantage of the 2D materials is that multiple layers can be stacked in the vertical direction so that the parallel combination of the edge modes further decreases the resistivity. For an interconnect with a cross section dimension smaller than 10nm, the multilayer Kagome lattice wire can outperform the Cu wire. The advantage is more significant as the size of the interconnect is further scaled down.

References

[1] P. Kapur, J. P. McVittie, and K. C. Saraswat, "Technology and reliability constrained future copper interconnects. I. Resistance modeling," *IEEE Trans. Electron Devices*, vol. 49, no. 4, pp. 590–597, Apr. 2002. doi: 10.1109/16.992867.

[2] H. Li, W.-Y. Yin, K. Banerjee, and J.-F. Mao, "Circuit modeling and performance analysis of multi-walled carbon nanotube interconnects," *IEEE Trans. Electron Devices*, vol. 55, no. 6, pp. 1328–1337, Jun. 2008. doi: 10.1109/TED.2008.922855.

[3] A. Naeemi and J. D. Meindl, "Conductance modeling for graphene nanoribbon (GNR) interconnects," *IEEE Electron Device Lett.*, vol. 28, no. 5, pp. 428–431, May 2007. doi: 10.1109/LED.2007.895452.

[4] L. Yang, C.-H. Park, Y.-W. Son, M. L. Cohen, and S. G. Louie, "Quasiparticle energies and band gaps in graphene nanoribbons," *Phys. Rev. Lett.*, vol. 99, no. 18, Nov. 2007, Art. no. 186801. doi: 10.1103/PhysRevLett.99.186801.

[5] L. Ye, M. Kang, J. Liu, F. von Cube, C. R. Wicker, T. Suzuki, C. Jozwiak, A. Bostwick, E. Rotenberg, D. C. Bell, L. Fu, R. Comin, and J. G. Checkelsky, "Massive dirac fermions in a ferromagnetic kagome metal," *Nature*, vol. 555, no. 7698, pp. 638–642, Mar. 2018. doi: 10.1038/nature25987.

[6] S. Nakatsuji, N. Kiyohara, and T. Higo, "Large anomalous Hall effect in a non-collinear antiferromagnet at room temperature," *Nature*, vol. 527, no. 7577, pp. 212–215, 2015. doi: 10.1038/nature15723.

[7] A. K. Nayak, J. E. Fischer, Y. Sun, B. Yan, J. Karel, A. C. Komarek, C. Shekhar, N. Kumar, W. Schnelle, J. Kübler, C. Felser, and S. S. P. Parkin, "Large anomalous Hall effect driven by a nonvanishing Berry curvature in the noncolinear antiferromagnet Mn_3Ge," *Sci. Adv.*, vol. 2, no. 4, Apr. 2016, Art. no. e1501870. doi: 10.1126/sciadv.1501870.

[8] H.-M. Guo and M. Franz, "Topological insulator on the kagome lattice," *Phys. Rev. B, Condens. Matter*, vol. 80, no. 11, Sep. 2009, Art. no. 113102. doi: 10.1103/PhysRevB.80.113102.

[9] C. L. Kane and E. J. Mele, "Quantum spin Hall effect in graphene," *Phys. Rev. Lett.*, vol. 95, Nov. 2005, Art. no. 226801.

[10] S. Datta, *Quantum Transport: Atom to Transistor*. Cambridge, U.K.: Cambridge Univ. Press, 2005.

[11] W. Steinhögl, G. Schindler, G. Steinlesberger, M. Traving, and M. Engelhardt, "Comprehensive study of the resistivity of copper wires with lateral dimensions of 100 nm and smaller," *J. Appl. Phys.*, vol. 97, no. 2, Jan. 2005, Art. no. 023706. doi: 10.1063/1.1834982.